PHYSICAL REVIEW A **92**, 041801(R) (2015)

Sensitivity of high-order-harmonic generation to aromaticity

A. F. Alharbi,[1,2] A. E. Boguslavskiy,[1] N. Thiré,[3] B. E. Schmidt,[3] F. Légaré,[3] T. Brabec,[1] M. Spanner,[4] and V. R. Bhardwaj[1,*]

[1]*Department of Physics, University of Ottawa, 150 Louis-Pasteur, Ottawa, Ontario, Canada K1N 6N5*

[2]*King Abdulaziz City for Science and Technology (KACST), P.O. Box 6086, Riyadh 11442, Saudi Arabia*

[3]*INRS-EMT, Advanced Laser Light Source, 1650 Lionel-Boulet Boulevard, Varennes, Canada J3X1S2*

[4]*National Research Council Canada, Ottawa, Ontario, Canada K1A 0R6*

(Received 26 May 2015; published 7 October 2015)

The influence of cyclic electron delocalization associated with aromaticity on the high-order-harmonic generation (HHG) process is investigated in organic molecules. We show that the aromatic molecules benzene (C_6H_6) and furan (C_4H_4O) produce high-order harmonics more efficiently than nonaromatic systems having the same ring structure. We also demonstrate that the relative strength of plateau harmonics is sensitive to the aromaticity in five-membered-ring molecules using furan, pyrrole (C_4H_4NH), and thiophene (C_4H_4S). Numerical time-dependent Schrödinger equation simulations of total orientation-averaged strong-field ionization yields show that the HHG from aromatic molecules comes predominantly from the two highest π molecular orbitals, which contribute to the aromatic character of the systems.

DOI: 10.1103/PhysRevA.92.041801 PACS number(s): 42.65.Ky, 33.20.Lg

Aromaticity is a manifestation of electron delocalization in cyclic molecules that influences their stability, reactivity, geometry, and interaction with external fields [1]. While it is widely used as a qualitative concept in chemistry to understand the behavior and structure of cyclic molecules, quantifying the degree of aromaticity of a molecule has been very challenging due to the lack of direct evaluation methods [2]. Different measures have been introduced in the literature to quantify aromaticity based on energetic, structural, magnetic, and electronic properties.

A widely utilized computational measure of aromaticity is the nucleus-independent chemical shift [NICS(1)] [3,4] that calculates the absolute magnetic shielding at 1 Å above the center of the ring. Another magnetic-based method beside NICS(1) is diamagnetic susceptibility (χ_G) [5]. The most common geometric-based measure is the harmonic oscillator model of aromaticity (HOMA) [6,7], which focuses on the tendency of aromatic molecules to display bond-length equalization. On the other hand, the energy-based measures of aromaticity, such as aromatic stabilization energy (ASE) [8], rely on the stability of the π electron systems. There are also other interesting schemes that link aromaticity to measurable observables based on molecular response properties, such as electric polarizabilities and hyperpolarizabilities and nuclear magnetic shieldings [9]. The different computational and experimental approaches of measuring aromaticity lead to different ordering of aromatic molecules [10,11]. This disagreement is due to the presence of competing effects beside electron delocalization that can influence the results of these methods. It is therefore essential to analyze aromaticity from different perspectives and extend it to newly explored dimensions for a better understanding of this long-fascinating subject.

In this Rapid Communication, we investigate the influence of aromaticity on high-order-harmonic generation (HHG) in some cyclic organic molecules. HHG in molecules is increasingly viewed as a promising spectroscopic tool with unprecedented spatial (angstrom) and temporal (attosecond) resolution. In this process, an intense laser field removes an electron from the parent molecule to the continuum where it gains energy and subsequently recombines with the parent ion, emitting a spectrum of high-energy photons [12].

Among the three distinct steps of HHG, ionization and recombination of the electron wave packet depend on the symmetry of the molecular orbitals and molecular structure, leaving their imprints on the harmonic spectrum. This has enabled one to probe (i) multiorbital interferences [13,14] and the Cooper minimum [15] by studying spectral modulations and (ii) molecular isomers by comparing harmonic amplitudes [16]. The main contribution to HHG in atoms comes from strong-field ionization (SFI) of the ground state and depends on the ionization potential. However, in molecules, HHG can be angle dependent [17], suppressed due to orbital symmetry [18,19], and can occur from multiple orbitals [13]. As a result, the ionization potential cannot be a good measure of the harmonic yield from molecules.

A longer wavelength of the laser field is desirable to generate HHG in molecules having a low ionization potential in the 8–11 eV range as it (a) ensures adiabatic ionization, (b) extends the cutoff harmonics to capture signatures of molecular and multielectron dynamics [15,20], (c) increases sensitivity to laser ellipticity, and (d) favors better phase matching at higher gas pressures [21]. With the availability of high-energy midinfrared light sources in the 1.4–4 μm wavelength region, there is renewed interest in extending HHG spectroscopy to complex polyatomic molecules.

Here we address two issues experimentally. (i) What is the influence of cyclic electron delocalization on HHG? Using short pulses and longer driving wavelengths, we produce and compare high harmonics in aromatic and nonaromatic molecules that have the same ring size and a similar atomic structure. In both six- and five-membered ring molecules we show that the HHG yield in aromatic molecules is up to an order of magnitude higher than in nonaromatic molecules. (ii) Is HHG sensitive to degree of aromaticity? For this part, we focus our study on the five-membered ring molecules

*ravi.bhardwaj@uottawa.ca

pyrrole (C_4H_5N), thiophene (C_4H_4S), and furan (C_4H_4O) that differ by a heteroatom. This is because (i) most measures of aromaticity are affected by the molecular size, making it difficult to compare molecules with different ring sizes [22], and (ii) the degree of aromaticity in these molecules was intensively investigated in the literature using different indicators. We show that the relative ratios of the plateau harmonics follow the same sequence proposed by most measures. Numerically, we investigate the contribution of π electrons to the enhancement of HHG emission in the studied aromatic compounds. It is the delocalization of these π electrons that is the central aspect of aromaticity.

The experiments were conducted at the Advanced Laser Light Source (ALLS) facility in Varennes, Canada. Harmonic emission was generated by focusing midinfrared (1825 nm, 50 fs) pulses into a finite gas cell (5 mm long with 0.6 mm apertures) using a 50 cm CaF_2 lens. The infrared pulses was first produced by an optical parametric amplifier pumped by a Ti:sapphire laser generating 45 fs pulses with an energy of 4.5 mJ and operating at a wavelength of 800 nm and a repetition rate of 100 Hz. The output beam is spatially filtered and then amplified by passing through a large Beta Barium Borate (BBO) crystal pumped by high-energy 800 nm light [23]. The energy of the amplified IR beam was varied from 200 μJ to 2 mJ by using a half-wave plate placed in front of a germanium plate. The emitted harmonics were spectrally dispersed by a flat-field concave grating at grazing incidence onto a microchannel plate detector coupled to a phosphor screen, where the image was captured by a charge-coupled device camera. The spectrometer and detection system were designed to capture high harmonics from about 17 eV onwards. Also, since the sensitivity of high-harmonic spectroscopy is in general high in the plateau and cutoff region of the harmonic spectrum, we do not record the low photon energy region. The spectrometer was calibrated by measuring the transmitted spectrum after an aluminum filter and the position of the Cooper minimum in argon [15]. The intensity of the laser beam was calibrated by monitoring the cutoff harmonics from harmonic emission in Ar and Xe. The molecular gas was introduced into the cell without utilizing a carrier gas. The molecules inside the gas cell were randomly oriented. Harmonics were optimized by varying the gas pressure and focal plane within the gas cell. All comparative measurements were done at the same gas density in a phase-matching regime which was in the order of 10^{17} cm^{-3}. In this regime, the ratios were found to be generally the same, even at different gas pressures. This suggests the observed differences between molecules is not due to phase-matching issues but due to the molecular response. All chemicals were obtained from Sigma-Aldrich with purities varying between 98% and 99%.

Benzene is emblematic of an aromatic system and is ranked as the most aromatic molecule, according to most measures. For example, the HOMA value of benzene is unity, which indicates that all bonds are equal in length. So, we compare the harmonic yields of benzene (C_6H_6) with nonaromatic molecules cyclohexene (C_6H_{10}) and cyclohexane (C_6H_{12}) that belong to the same family of six-membered rings, as shown in Fig. 1(a). All three molecules have approximately similar ionization potentials (9.25, 8.94, and 10.32 eV, respectively [24]) and the harmonics are produced

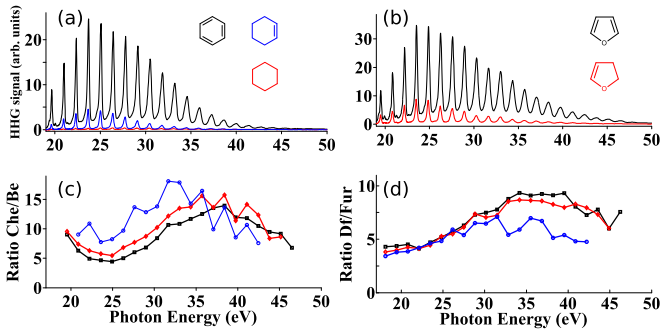

FIG. 1. (Color online) HHG spectra for (a) benzene (black), cyclohexene (blue), and cyclohexane (red) obtained using 1825 nm light at an intensity of 6.5×10^{13} W/cm^2. (b) For furan (black) and 2,3-dihydrofuran (red) obtained using 1825 nm light at an intensity of 4.5×10^{13} W/cm^2. (c), (d) Cyclohexene-to-benzene signal and 2,3-dihydrofuran-to-furan signal at three different intensities: 4.5 (blue circle), 6.5 (red diamond), and 8.6 (black square) in units of 10^{13} W/cm^2.

at an intensity of 6.5×10^{13} W/cm^2 and identical pressures in the gas cell. The harmonic signal from benzene is greater by a factor of 8 and 20 compared to cyclohexene and cyclohexane, respectively. The harmonic signal from benzene also exceeds that of other six-membered ring molecules 1,3 cyclohexadiene and 1,4 cyclohexadiene (not shown). Figure 1(c) shows the ratio of harmonic signal from benzene to that of cyclohexene as a function of harmonic energy for three different intensities. Although the ratios are different in magnitude, their dependence on harmonic order is similar, indicating that significant differences are present between aromatic and nonaromatic molecules over a large range of laser intensities. While the ratio for lower-order harmonics varies with intensity, it is nearly independent for plateau and cutoff harmonics. Previous studies on HHG in benzene and cyclohexane [25] using an 800 nm driving field with 70 and 240 fs pulses only produced lower-order harmonics with the harmonic yield of benzene higher by a factor of 2–4 than that of cyclohexane.

To ensure that higher-harmonic yields in aromatic molecules are universal, we studied HHG in five-membered ring molecules. Figure 1(b) shows the harmonic spectrum for aromatic furan (C_4H_4O) and nonaromatic 2,3-dihydrofuran (C_4H_5O) at an intensity of 4.5×10^{13} W/cm^2. These two molecules have ionization potentials of 8.88 and 8.55 eV, respectively [26]. Figure 1(d) shows their ratio for different intensities. The harmonic signal in furan is up to an order magnitude higher than its nonaromatic counterpart, and the ratio is nearly independent of laser intensity over the entire harmonic range except for the lowest intensity, where the ratio decreases for high-energy photons.

To further understand the origin of the HHG yield enhancement in aromatic molecules, we performed time-dependent numerical calculations of the SFI yields from different molecular orbitals. We calculated the half-cycle SFI, which reflects the subcycle SFI yields that are relevant to the first step of the subcycle HHG process. Computations are carried out using the time-dependent resolution-in-ionic-states (TD-RIS) method outlined in Ref. [27] (see the Appendix for further details about the SFI calculations). The top row of Fig. 2 shows the

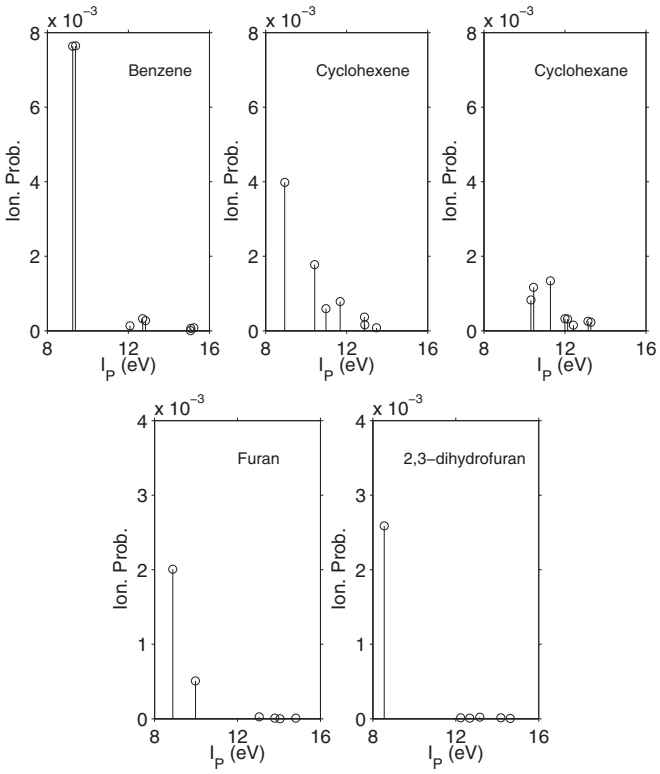

FIG. 2. Top row: Half-cycle ionization probabilities for the lowest eight cation states of benzene, cyclohexene, and cyclohexane at an intensity of 6.5×10^{13} W/cm^2. (Note: A small shift of 0.1 eV was added to one component of the degenerate states in benzene and cyclohexane to help make these states distinguishable in the plots.) Bottom row: Half-cycle ionization probabilities for the lowest few cation states of furan and 2,3-dihydrofuran at an intensity of 4.5×10^{13} W/cm^2. Probabilities were calculated for a laser wavelength of 1825 nm.

half-cycle SFI probabilities for ionization to the lowest few cation states of benzene, cyclohexene, and cyclohexane. The highest occupied molecular orbital (HOMO) of benzene is a π orbital and is doubly degenerate. The first two channels in benzene corresponding to HOMO ionize significantly compared to other channels and contribute coherently to HHG. In cyclohexene and cyclohexane, ionization is lower than in benzene and occurs from multiple orbitals.

From our calculations, the total ionization yield (summation over the yield for all the cation channels of each molecule) of benzene is ∼2 and ∼3.5 times larger than the total yields of cyclohexene and cyclohexane, respectively. This is in agreement with previous observations of saturation intensities (a measure of the ionization efficiency) for benzene and cyclohexene [28]. Also, the relative photoionization cross section for cyclohexane was found to be 15% of benzene at 780 nm [29]. The observed differences in numerical ionization yields will translate to an even higher difference in the HHG signal when the recombination step and dynamical interferences from multiple orbitals in cyclohexene and cyclohexane are taken into account [13]. This suppression effect in the case of multiple active HHG channels will be common to HHG in all complex molecules involving closely spaced multiple orbitals.

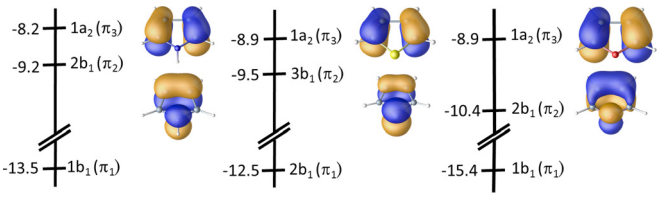

FIG. 3. (Color online) Experimental binding energies for π molecular orbitals of pyrrole (left), thiophene (middle), and furan (right) [30]. The Dyson orbitals corresponding to the two highest ionization channels are also shown.

The bottom two panels in Fig. 2 show the ionization probability in the five-membered ring molecules furan and 2,3-dihydrofuran. Differences in ionization exist but are not as profound as in six-membered ring molecules. The total ionization probabilities for the two species are essentially equal. In furan, HOMO-1 contributes by about 20% to the total ionization, whereas in 2,3-dihydrofuran no orbital other than the HOMO contributes to ionization. However, the fact that experimental harmonic yields in furan are a factor of 4–10 higher than 2,3-dihydrofuran over a range of harmonics suggests that, on a quantitative level, the recombination step plays a significant role in the observed harmonic yields.

We now focus on the differences in the HHG yield among aromatic molecules to see how they could be connected to the degree of aromaticity. To minimize the influence of other factors, we compare the HHG in furan (C_4H_4O), pyrrole (C_4H_4NH), and thiophene (C_4H_4S). These three molecules are considered to be the archetype of five-membered heteroaromatic compounds and they all share similar geometric, atomic, and electronic structures. They have comparable ionization potentials of 8.88, 8.20, and 8.86 eV [26], respectively. Since there are six π electrons in these aromatic molecules, one from each carbon atom and two from the unshared pair on the heteroatom, the first two occupied π orbitals (π_3 and π_2) represent HOMO and HOMO-1 (Fig. 3). These orbitals have the same general shape in all three molecules but differ slightly in their localization properties. The lowest-lying π_1 orbital represents HOMO-4 in pyrrole, HOMO-3 in thiophene, while it is HOMO-6 in furan. According to most descriptors of aromaticity, furan is least aromatic among the three molecules. However, between thiophene and pyrrole there is no consensus on which of these molecules is more aromatic. ASE and χ_G [11] measures consider pyrrole to be more aromatic than thiophene, whereas according to NICS(1) [31] measure thiophene is more aromatic. Other versions of NICS [1,22] indicate a classification that agrees with ASE and χ_G. On the other hand, the HOMA [11] index gives comparable values for both molecules.

Figure 4(a) shows the ratio of the harmonic signal of pyrrole to furan for three different intensities at 1825 nm. A ratio of unity indicates both molecules have the same harmonic yields. At the lowest intensity of 2.5×10^{13} W/cm^2, the harmonic signal in pyrrole is higher by a factor of 3–4. The ratio decreases for higher-order harmonics close to the cutoff. The high fluctuations of the ratio are due to the low-harmonic signal as a result of low gas densities (restricted by the low vapor pressure of pyrrole) and laser intensity. At higher intensities,

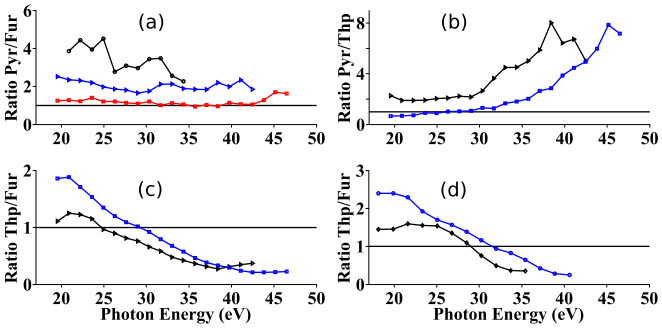

FIG. 4. (Color online) Ratio of harmonic signals. (a) Pyrrole to furan using 1825 nm at three different laser intensities: 2.5 (black circle), 4.5 (blue triangle), and 6.5 (red square) in units of 10^{13} W/cm^2. (b) Pyrrole to thiophene, and (c) thiophene to furan using 1825 nm at two different laser intensities: 4.5 (black triangle) and 6.5 (blue square) in units of 10^{13} W/cm^2. (d) Thiophene to furan using 1430 nm at two different laser intensities: 4.5 (black diamond) and 6.5 (blue circle) in units of 10^{13} W/cm^2.

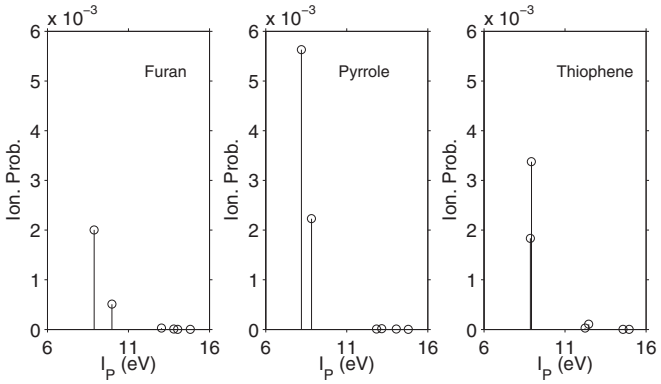

FIG. 5. Ionization probabilities for the calculated lowest six cation doublet states of pyrrole, thiophene, and furan using 1825 nm laser pulses at an intensity of 4.5×10^{13} W/cm^2 over a period of a half laser cycle.

the ratio remains nearly constant for both plateau and cutoff harmonics. However, the ratio decreases with intensity since pyrrole ionizes faster and reaches saturation at lower intensities than furan. Saturation in pyrrole occurs at $\sim 6 \times 10^{13}$ W/cm^2 while in furan it occurs at $\sim 10^{14}$ W/cm^2.

Figure 4(b) shows the ratio of the harmonic signal of pyrrole to thiophene for two different intensities at 1825 nm. At an intensity of 4.5×10^{13} W/cm^2, the pyrrole signal is a factor of 2 higher than thiophene for lower harmonics. At 6.5×10^{13} W/cm^2, lower-order harmonics in the recorder spectra for both molecules produce a similar harmonic signal but pyrrole starts to dominate for the rest of plateau harmonics. At both intensities, the ratio increases beyond 30–35 eV. A possible explanation for this decline in the thiophene signal can be linked to the presence of a Cooper minimum. A previous study showed that the HHG spectra of molecules containing atoms such as sulfur can exhibit a Cooper minimum at around 42 eV [15]. In thiophene spectra, the minimum cannot be clearly observed because it is close to the cutoff harmonics, which are relatively lower due to a low ionization potential. However, it could significantly weaken the already decaying signal.

Figures 4(c) and 4(d) show the ratio of the harmonic signal of thiophene to furan at 1825 and 1450 nm, respectively, for two different intensities; 4.5×10^{13} and 6.5×10^{13} W/cm^2. At the lower intensity, only the lower sides of the harmonic plateaus have higher yields in thiophene compared to furan. At the higher intensity, the thiophene domination extends to more plateau harmonics, however, closer to the potential Cooper minimum, the harmonic signal from furan is higher at all intensities. This behavior is wavelength independent.

Our results on high-harmonic yields in five-membered aromatic molecules suggest pyrrole to be more efficient at producing plateau harmonics, followed by thiophene and then furan. This ordering agrees with many aromaticity measures such as ASE and diamagnetic susceptibility. To confirm our findings, we calculated the ionization probabilities of the highest orbitals in all three molecules, as shown in Fig. 5. A common signature of all three aromatic molecules is that essentially all of the subcycle ionization comes from the two highest π orbitals. In pyrrole, ionization from HOMO is dominant, with about 30% of the total ionization yield coming from HOMO-1. The total ionization of pyrrole is three times that of furan. The observed differences in ionization of pyrrole and furan are in reasonable agreement with the experimental harmonic yields shown in Fig. 4(a). In thiophene, HOMO-1 is the dominant channel, with HOMO contributing only 35% of the total ionization yield. In furan, ionization from HOMO is a factor of 4 larger than that of HOMO-1. The total ionization yield for thiophene is two times larger than the total yield for furan, which reflects the observed harmonic yields without invoking the recombination step, except for the harmonics closer to the cutoff in thiophene, as discussed earlier.

We conclude that the efficiency of producing high harmonics in organic cyclic molecules is sensitive to aromaticity, which could add more insight into the understanding of this subject. The observed link between aromaticity and HHG can be understood from the fact that the highest π orbitals are mainly responsible for the enhanced HHG emission in aromatic molecules. This property is remarkable since several existing aromaticity measures cannot decouple the contribution of σ orbitals from the description of aromaticity [1,32]. However, the HHG process does not probe the entire π molecular orbital system and is influenced by other factors such as multiorbital effects and electronic structure. As a result,

TABLE I. Parameters used in the MCSCF calculations for each molecule: number of active electrons, number active orbitals, and number of states included in the state-averaged variational solution.

Molecule	Active electrons, cation (neutral)	Active orbitals	States in average
Benzene	29 (30)	17	8
Cyclohexene	13 (14)	8	7
Cyclohexane	35 (36)	18	8
2,3-dihydrofuran	13 (14)	8	6
Furan	25 (26)	15	6
Pyrrole	25 (26)	15	6
Thiophene	7 (8)	7	6

TABLE II. Ionization potentials (IPs) used in the SFI simulations. The IPs from the ground state of the neutral to the ground state of the cations were set to the available experimental values [24,26,34]. The IPs of the excited cation states were calculated by starting with the experimental D_0 IP and then adding the computed excitation energies.

State	Benzene	Cyclohexene	Cyclohexane	2,3-dihydrofuran	Furan	Pyrrole	Thiophene
D_0	9.25	8.94	10.32	8.55	8.88	8.20	8.86
	9.25		10.32				
D_1	12.08	10.42	11.28	12.24	9.98	8.83	8.93
D_2	12.71	10.98	12.00	12.67	13.04	12.84	12.24
	12.71		12.00				
D_3	15.07	11.68	12.42	13.16	13.79	13.16	12.47
D_4	15.09	12.87	13.14	14.17	14.05	14.07	14.58
	15.09		13.14				
D_5		12.89		14.62	14.82	14.79	14.95
D_6		13.48					

it cannot be used to conclusively characterize aromaticity. Similar limitations were also observed in many well-known approaches to study aromaticity, such as HOMA. For example, it was shown that some nonaromatic cyclic compounds and many acyclic systems have bond-length equalized structures [1].

The authors wish to acknowledge A. Laramee for expert technical assistance.

APPENDIX: COMPUTATIONAL METHODS

The field-free multielectron states were obtained using the GAMESS electronic structure code [33] using the augmented correlation-consistent polarized valence double zeta (aug-cc-pVDZ) basis set. The neutral geometries for all species were optimized at the restricted Hartree-Fock second-order Møller-Plesset (RHF MP2) level of theory. The neutral singlet and ionic double electronic states were then recalculated at these geometries using the complete-active-space multiconfigurational self-consistent field (CAS-MCSCF) level of theory. All relevant parameters for the CAS computations are given in Table I. The ionic states used in the calculations for each molecule along with their ionization potentials are shown in Table II.

The SFI is computed using the time-dependent resolution-in-ionic-states (TD-RIS) method outlined in Ref. [27]. The continuum wave packets are represented on Cartesian grids. The grids extend from to ± 15 atomic units (a.u.) in all directions with a grid spacing of 0.2 a.u. Absorbing boundary conditions [35] are used in all directions with a width of 4.4 a.u. from the boundary edges. The ionic-channel-resolved SFI yield was calculated by monitoring the density absorbed at the boundaries of the continuum grids for each ionic channel. The calculation of the SFI yields used a single half cycle of the ionizing laser field

$$\vec{F}(t) = \vec{e}_F \begin{cases} F_0 \sin(\omega t), & 0 < t \leqslant \tau/2, \\ 0, & t > \tau/2, \end{cases} \tag{A1}$$

where $\vec{e}_F$ is the laser polarization direction, $\omega = 0.025$ a.u. (1825 nm), $\tau = 2\pi/\omega$ is the period of the carrier oscillations, and F_0 is the peak electric field of the laser. The peak intensities used in the computations are given above for each particular case. The time integration was carried out over the range $t =$ 0–200 a.u. This leaves an additional 45 a.u. after the half cycle is over to give the liberated electron wave function time to be absorbed at the grid edge. The time step used for propagation was $\Delta t = 0.002$ a.u. The SFI yields were averaged over all angles between the molecular frames and the laser polarization $\vec{e}_F$. The averaging was carried out using angular Lebedev grids of the ninth order.

[1] Z. Chen, C. S. Wannere, C. Corminboeuf, R. Puchta, and P. V. R. Schleyer, Chem. Rev. **105**, 3842 (2005).
[2] F. Feixas, E. Matito, J. Poater, and M. Solà, Chem. Soc. Rev. **44**, 6434 (2015).
[3] P. V. R. Schleyer, C. Maerker, A. Dransfeld, H. Jiao, N. J. R. V. E. Hommes, D. Erlangen, and R. V. February, J. Am. Chem. Soc. **7863**, 6317 (1996).
[4] P. V. R. Schleyer, M. Manoharan, Z.-X. Wang, B. Kiran, H. Jiao, R. Puchta, and N. J. R. van Eikema Hommes, Org. Lett. **3**, 2465 (2001).
[5] J. Aihara, J. Am. Chem. Soc. **128**, 2873 (2006).
[6] J. Kruszewski and T. M. Krygowski, Tetrahedron Lett. **13**, 3839 (1972).
[7] T. M. Krygowski, J. Chem. Inf. Comput. Sci. **33**, 70 (1993).
[8] W. J. Hehre, R. T. McIver, Jr., J. A. Pople, and P. v. R. Schleyer, J. Am. Chem. Soc. **6901**, 7162 (1974).
[9] P. Lazzeretti, Phys. Chem. Chem. Phys. **6**, 217 (2004).
[10] J. Poater, I. García-Cruz, F. Illas, and M. Solà, Phys. Chem. Chem. Phys. **6**, 314 (2004).
[11] K. Najmidin, A. Kerim, P. Abdirishit, H. Kalam, and T. Tawar, J. Mol. Model. **19**, 3529 (2013).
[12] P. B. Corkum, Phys. Rev. Lett. **71**, 1994 (1993).
[13] O. Smirnova, Y. Mairesse, S. Patchkovskii, N. Dudovich, D. Villeneuve, P. Corkum, and M. Y. Ivanov, Nature (London) **460**, 972 (2009).
[14] H. J. Wörner, J. B. Bertrand, P. Hockett, P. B. Corkum, and D. M. Villeneuve, Phys. Rev. Lett. **104**, 233904 (2010).
[15] M. C. H. Wong, A.-T. Le, A. F. Alharbi, A. E. Boguslavskiy, R. R. Lucchese, J.-P. Brichta, C. D. Lin, and V. R. Bhardwaj, Phys. Rev. Lett. **110**, 033006 (2013).
[16] M. C. H. Wong, J.-P. Brichta, M. Spanner, S. Patchkovskii, and V. R. Bhardwaj, Phys. Rev. A **84**, 051403 (2011).

[17] N. Hay, R. Velotta, M. Lein, R. de Nalda, E. Heesel, M. Castillejo, and J. P. Marangos, Phys. Rev. A **65**, 053805 (2002).
[18] J. Muth-Böhm, A. Becker, and F. H. M. Faisal, Phys. Rev. Lett. **85**, 2280 (2000).
[19] B. Shan, X.-M. Tong, Z. Zhao, Z. Chang, and C. D. Lin, Phys. Rev. A **66**, 061401(R) (2002).
[20] R. Torres, T. Siegel, L. Brugnera, I. Procino, J. G. Underwood, C. Altucci, R. Velotta, E. Springate, C. Froud, I. C. E. Turcu *et al.*, Phys. Rev. A **81**, 051802 (2010).
[21] T. Popmintchev, M.-C. Chen, O. Cohen, M. E. Grisham, J. J. Rocca, M. M. Murnane, and H. C. Kapteyn, Opt. Lett. **33**, 2128 (2008).
[22] M. Alonso and B. Herradón, J. Comput. Chem. **31**, 917 (2010).
[23] N. Thiré, S. Beaulieu, V. Cardin, A. Larame, V. Wanie, B. E. Schmidt, and F. Légaré, Appl. Phys. Lett. **106**, 091110 (2015).
[24] K. Kimura, S. Katsumata, Y. Achiba, T. Yamazaki, and S. Iwata, *Handbook of HeI Photoelectron Spectra of Fundamental Organic Molecules* (Halsted Press, New York, 1981).
[25] N. Hay, M. Castillejo, R. de Nalda, E. Springate, K. J. Mendham, and J. P. Marangos, Phys. Rev. A **61**, 053810 (2000).
[26] P. Linstrom and W. Mallard, *NIST Chemistry WebBook, NIST Standard Reference Database Number 69* (National Institute of Standards and Technology, Gaithersburg, MD) (retrieved April 26, 2015), http://webbook.nist.gov.
[27] M. Spanner and S. Patchkovskii, Phys. Rev. A **80**, 063411 (2009).
[28] S. M. Hankin, D. M. Villeneuve, P. B. Corkum, and D. M. Rayner, Phys. Rev. A **64**, 013405 (2001).
[29] M. J. DeWitt and R. J. Levis, J. Chem. Phys. **108**, 7045 (1998).
[30] J. Eland, Int. J. Mass Spectrom. Ion Phys. **2**, 471 (1969).
[31] K. E. Horner and P. B. Karadakov, J. Org. Chem. **78**, 8037 (2013).
[32] S. Pierrefixe and F. Bickelhaupt, Chem. Eur. J. **13**, 6321 (2007).
[33] M. W. Schmidt *et al.*, J. Comput. Chem. **14**, 1347 (1993).
[34] K. Bernhard, J. Geimer, M. Canle-Lopez, J. Reynisson, D. Beckert, R. Gleiter, and S. Steenken, Chem. Eur. J. **7**, 4640 (2001).
[35] D. Manolopoulos, J. Chem. Phys. **117**, 9552 (2002).